

# A New Synthetic Training Environment System Based On An ICT-Approach For Manual Ultrasonic Testing

Alvin Yung Boon Chong<sup>1</sup>, Abdeldjalil Bennecker<sup>1</sup>, Fredrik Hagglund<sup>2</sup>, Saarim Siddiqi<sup>1</sup>, Vassilios Kappatos<sup>1</sup>,  
Cem Selcuk<sup>1</sup> and Tat-Hean Gan<sup>1</sup>

<sup>1</sup>Brunel Innovation Centre, Brunel University, Abington Hall, Granta Park, Great Abington, Cambridge, CB21 6AL, United Kingdom

<sup>2</sup>TWI Ltd, Granta Park, Great Abington, Cambridge, CB21 6AL, United Kingdom

Email Address: alvin.chong@brunel.ac.uk

## Abstract

Training to qualify as a manual ultrasonic inspector takes a long time and costs a considerable amount of money. We developed a virtual training environment using an innovative dead-reckoning optical sensor that yields translational position which offers additional information to operators and examiners alike. The training environment contains a library of test scenarios, shows surface coverage, measures the time of inspection, indicates detected defects and provides a performance score. Our test-bed trial results using a pool of Ultrasonic Test (UT) qualified and unqualified participants on two virtual training blocks that contain 2 flaws each reveal 100% detection and an accuracy of 5 mm in locating defects in more than 50% of the measured defect locations.

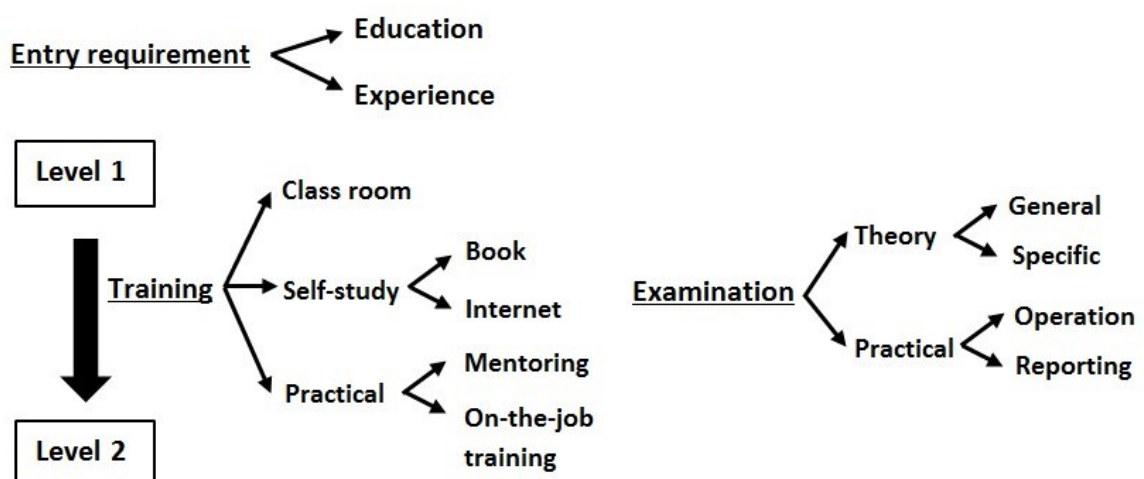
**Keywords:** ultrasonic, probability of detection, synthetic training, information and communication technology, optical sensor and tracking system.

## 1. Introduction

Manual Ultrasonic Testing (MUT) is a well-established and widely adopted Non-destructive Testing (NDT) technique in engineering industry. However, the reliability of a MUT system depends primarily on the capability of its key components which mainly comprise of the procedure, the equipment and the personnel. While improvements in the former two elements have received considerable attention amongst different research communities, the latter mainly benefited from comprehensive investigations on the influence of human factors affecting the Probability of Detection (PoD) [1-4]. Moreover, a salary survey conducted by Personnel for Quality and Non-destructive Testing (PQNNDT) in 2013 revealed that the average age for an NDT technician is 46 years old. This is an increase of 3.5 years since 2006 when a similar survey has taken place [5]. This indicates that the existing NDT workforce has an aging demography which creates a severe shortage of skilled personnel. The increased complexity of

equipment, particularly in ultrasonic testing, and the introduction of new techniques have also led to a higher number of training hours and more stringent qualification for NDT operators. Certification of personnel has been established in the NDT industry for nearly 40 years but the process is still protracted, arduous and expensive. On the contrary, synthetic training simulators have been developed in broad range of applications such as, for aviation, shipping, military and healthcare, particularly, where high performance and reliability are critical. Yet, most MUT operator training and examination, to this date, still rely on traditional ways of teaching without much recourse to modern Information and Communication Technology (ICT) tools.

Typically, NDT inspectors are required to be qualified in accordance with a recognised programme with pre-requisites to satisfy prescribed requirements for a combination of education, training and experience. This aims to ensure that the trainee has the potential to understand the principles and procedures of the applicable NDT methods. As an example, an ultrasonic inspector will be required to have attended a training course of 120 hours duration and to have gained 12 months experience working under the supervision of already qualified staff. The content and duration of the training course along with the format of the examination are typically in accordance with standards such as EN4179 and NAS410 [6,7]. In almost all NDT practical examinations, the candidates should test a number of components, containing a certain number of defects and to report any indications above a nominal size (i.e. based on acceptance criteria) in a predetermined period of time. They will be further required to classify these defects according to type and report their dimensions and locations. The diagram in figure 1 illustrates a typical training path for training NDT operators, showing the stringent requirements. As a consequence, the development of synthetic training environment that reduces the number of hours required for certification and provides detailed information about the operator performance is highly desirable.



Despite the importance of training simulators in the field of NDT [8-12] and the need for low-cost UT pieces containing complex defects [13], the literature in these subjects are limited. The first attempt to introduce the concept of synthetic environment training in the field of NDT was made by Harris and

**Figure 1.** Typical certification and qualification path for NDT equipment operators.

Spanner Jr, in 1999 for ultrasonic testing [8]. Subsequently, Haritos and Macchiarella developed a mobile augmented reality system for aerospace visual inspection training [14]. They demonstrated that it reduces the training time and cost whilst supplies rapid and accurate feedback. In a similar trend, De Crescenzo *et al* proposed augmented reality for aircraft maintenance and operations support using a markerless camera pose estimation [15]. The contribution of the Southwest Research Institute to the subject of simulators in NDT was summarised by Dowing *et al* [16]. They discussed the capabilities of their AutoGrid, Eddy Current and borescope simulators.

One key NDT technique is MUT. It is simple, cost effective, quick to deploy and easy to use. However, it requires more training hours than other conventional NDT techniques such as visual inspection. MUT technique involving hand-to-eye coordination is perceived to benefit more from these Synthetic Training Environments (STE) than techniques relying on image interpretations such as automated ultrasonic test. There may also be limitation to utilise robots in areas of difficult access (i.e. awkward position and small opening). The development of a training simulator which can provide more details about an inspection to an operator is highly desirable as currently, score of the examination are typically limited to the relative number of correctly reported indications of discontinuities and false alarm in the test specimen. The flaws found are then characterised in terms of location, size and type. These parameters are appropriate and useful but they provide only information about the overall performance of the operator and very little information about the adequacy of the process employed by the operator in conducting the examination. In this paper, a STE system suitable for NDT operator training is proposed. The advantages of the proposed STE system are, (i) it complements conventional approaches to the training and assessment of MUT operators by providing additional inspection features in a cost effective way and (ii) it provides digitally created substitutes for the test pieces (with and without flaws) required for NDT training and examination. This is beneficial since samples of specimens from actual site taken from aircraft, nuclear plants or specimens manufactured specifically for testing purposes can be expensive. In addition, some components can be very large which would require special handling and large storage facilities. There can also be safety concerns in some cases where the specimens are from an operational nuclear plant and consequently restricted access to the facility. It is envisaged that using a combination of synthetic and real training system can enhance the effectiveness and reduce the costs of training and assessment of operator. Consequently, it is anticipated that one measure of success would be the acceptance of this proposed

STE system as part of the formal training programmes for MUT qualifications and standards implemented worldwide. This could also be followed by regulations to ensure universal consistency in different applications.

The STE system aimed to provide additional information to manual operators such as surface coverage, time of inspection and defects indication. The validation of the STE system was performed via a trial

conducted by a participant pool consisting of 3 qualified/experienced and 3 unqualified MUT inspectors on representative industry standard test pieces (flat steel blocks) containing well characterised flaws (flat bottom holes), with locations unknown to the participants. Typical performance variables used in NDT such as PoD, coverage, inspection efficiency were taken for each system. The trial results based on the performance variable indicate that the proposed STE system demonstrates an encouraging results in which the unqualified and inexperienced personnel achieved standard competency in a short period.

## 2. The architecture of the proposed STE System

The flow diagram of the STE system is shown in figure 2 The system allows the trainee to step through the procedure by pressing on-screen buttons while following the instructions on the screen. This acts as a substitute for the long and complicated inspection manuals currently in practice. The STE procedures can be described as follow,

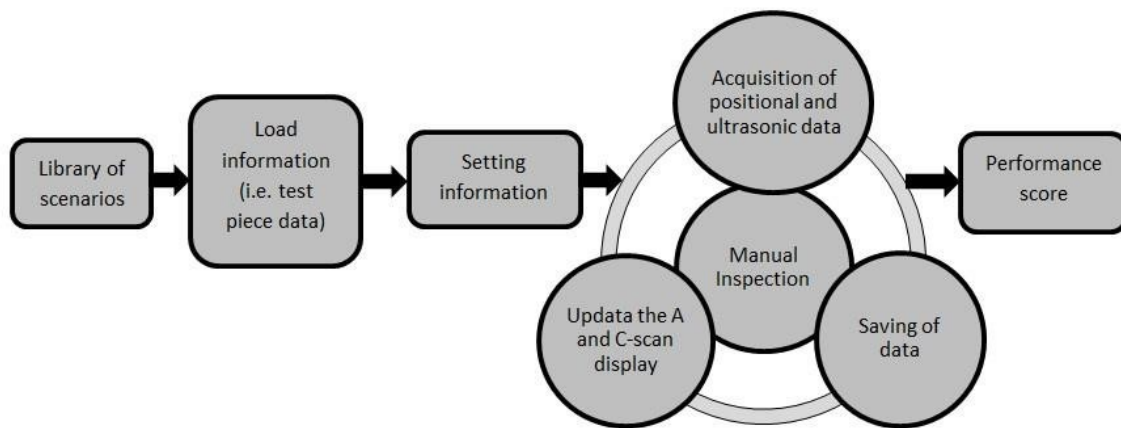


**Figure 2.** Flow diagram showing the concept of STE system.

### *STEP 1: Load information*

The trainee is able to load information about the test piece and its corresponding ultrasonic data from a library of scenarios. These data can either be pre-collected using existing UT equipment or produced by simulation. The entire matrix of ultrasonic amplitude signals at all locations will be loaded.

### *STEP 2: Setting Information*

The settings window will be shown on the screen to simulate probe calibration procedure.

### *STEP 3: Manual inspection*

Trainee begins the inspection; the STE system will be able to track the movement of the probe position in a pre-defined reference frame. The A-scan and the C-scan are simultaneously displayed on the screen in real time to guide the trainee. The option of saving the trainee's data is also made available.

#### *STEP 4: Performance score*

The performance score (i.e. PoD, coverage and inspection efficiency) can be generated after the completion of the manual inspection.

Test pieces are pivotal for evaluating NDT techniques, assessing NDT inspectors or conducting large trials. In the ideal training environment, a large number of operators can inspect the same test piece containing simple and complex defects either simultaneously or consecutively. This also allows statistically valid results to be obtained and conclusions to be drawn from the significant amount of data that can be collected. There is already a need for a shared database of real test pieces between researchers, NDT training schools and industries [13]. Real specimens can be difficult to obtain or manufacture. They may also be hazardous or too large for practical storage. On the other hand, virtual test pieces can offer a real alternative. They are easy to store, transfer and maintain the security of the information they contain. It is worth mentioning that the library of test scenarios depends to some extent on the acquisition of data from real specimens for which the true conditions must be determined. In the event where real specimens are unavailable, instructors or test specialists are able to develop new virtual test pieces by modifying or combining the raw data from several test pieces already in existence. The signal can be artificially modified for operator practice or testing purposes by simply changing certain characteristics of the signal, such as the amplitude or signal-to-noise ratio.

### **3. Implementation of the STE System**

There are basically 2 sources of information available, (i) the two translational data obtained from the optical sensor and (ii) the ultrasonic data obtain by the ultrasonic probe, figure 3. In terms of the position, two degrees of freedom can then be achieved in a pre-defined body frame. The main objective in the interfacing section is to build an integrated system to obtain data from each of the individual sensor and manipulate it to achieve a meaningful representation for the MUT trainee. A data acquisition system is required to establish a bidirectional communication between different sensors and the STE operating system.

To implement the acquisition system, Arduino Bluetooth module is selected. Translational data are acquired from the sensor denoted by ■ and ■ and the ultrasonic data denoted with ■. This yields the position (■ and the ultrasonic data (■) which can be read directly to the STE system via the ultrasonic device's Dynamic-Link Library (DLL) provided by the manufacturer.

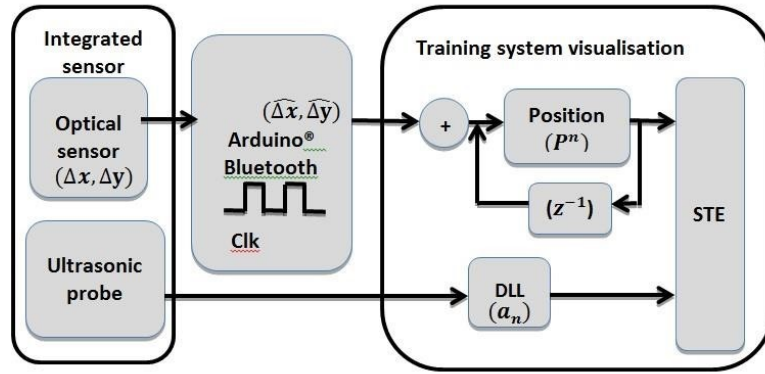


Figure 3. Data communication flow for the STE system.

### 3.1 Dead-reckoning spatial positioning system

An optical sensor has been investigated to determine its suitability as an element for a deadreckoning spatial position module for the STE system. In term of the optical sensing based odometer, designs have been reported employing the principles of time-of-flight [17], interferometry [18] and triangulation [19]. Owing to its common usage, this technique could possibly be well received since many are already familiar with its use. The demands of computer usage have grown increasingly over the years and this has led to improvements in the optical sensor particularly in delivering the higher tracking speed, better response and reliability required. Optical mouse is also immune to the problems of wear and dirt accumulation. Optical mice rarely need cleaning, track precisely up to sub-micron accuracy [20] and work on nearly all surfaces including curved surfaces (large radius) and soft fabric. Combining optical approaches with advances in signal/image processing, solid state electronics and wireless communication technologies, it is possible to achieve a small, cordless, high performance and inexpensive optical odometer.

Typically an optical mouse module consists of a single light source such as Light-Emitting Diode (LED) or sometime laser, lens for focusing and a Complementary Metal-Oxide-Semiconductor (CMOS) sensor located in the integrated circuit chip encased [21]. When the light source illuminates the surface at an angle underneath the mouse, the light reflected off microscopic textural features in the illuminated region which subsequently focused by the clear plastic lens to the CMOS to produce an image. The CMOS comprises of two-dimensional arrays pixel capture the images at a very fast scanning rate (700 frames per second or more) in order for the successive images to overlap. An optical navigation engine (feature extraction software) is then used to process the optical data collected and calculates the distance between successive images. This relative distance information is translated into x and y coordinates to indicate the displacement from the previous position.

It is worth mentioning that errors may be introduced when certain conditions occur during the operation of the optical sensor. These errors can be broadly classified under two main categories: systematic and

non-systematic errors. Systematic errors are intrinsic noise accumulated due to rereferencing of the reference frame during the operation of the sensor [22]. This arises because at some point in the movement of the optical sensor, the successive image which is to be compared with the reference image may no longer overlap the reference image to a degree sufficient to be able to accurately identify the motion of the sensor. Consequently, due to the lack of absolute positional reference, at each re-referencing, any positional errors from the previous re-referencing procedure are inherently accumulated. The amount of measurement error over a given distance can be statistically expressed as:

$$\text{Error} = \epsilon \cdot N \quad (1)$$

Where  $\epsilon$  = error per reference frame update and

$N$  = number of reference frame updates for the total distance travelled.

The systematic error will work out to be negligible using the proposed optical sensor based on the following assumptions. (i) Re-referencing may need occur each time the sensor moves 50% of the pixels which corresponds to one reference frame update every 0.5 mm. (ii) Assuming  $\epsilon$  has an error of half pixel size (25  $\mu\text{m}$ ). The error works out to be 4.3 mm for a total scanning length of 15 m.

The three known type of non-systematic errors have the following causes: (i) homogeneous surface features, (ii) heading and (iii) large lift-off distance. When the optical sensor moves along a homogeneous surface, successive identical micro texture images will be collected causing the optical sensor to appear to be stationary. This may be overcome by higher resolution of the optical sensor or may be reduced by means of calibrating the sensor to the material surface [23] as carried out in the next section. The error due to heading implies that when the optical sensor moves along an arc of length, it measures always the identical values independently from the radius of the arc. Thus, this means that the operator will have to keep the sensor orientation the same throughout the inspection for the results to be accurate. Error due to large lift-off distance will not be significant since MUT is a contact method. For rapid prototyping, an optical sensor from a low cost optical computing mouse is used. This consists of a low power, small form factor optical sensor, ADNS-5090 (PixArt) [24]. The operating voltage ranges from 2.8 – 3.7 V and a power management mode is also available which is ideal for power sensitive applications. This can be powered with a 3.7 V Lithium-Polymer rechargeable battery. The optical sensor is capable of high speed motion detection of up to 7.62 m/s. The resolution selected is 40 count/m (CPM) for this particular chip. The optical sensor comprises of 19 x 19 pixels. The physical individual pixel size is 40  $\mu\text{m}$  however the lens has a magnification of 1: 1.25, therefore each pixel will be seen as 50  $\mu\text{m}$  size on the surface, corresponding to a pixel array area of 0.9025  $\mu\text{m}^2$ . The sensor takes pictures at 2250 frames per second, which is fast enough to ensure that sequential pictures overlap. Based on

available open source information [25], it is possible to read the relative x and y positions obtain by the optical sensor.

### 3.2 Optical sensor experiment

In order to validate the accuracy of the proposed optical odometer, an extensive calibration and experimental investigation was carried out. The optical sensor was attached to the arm of the 3D linear stage scanner such that the plane axes of the optical sensor were parallel to the surface of the material specimens. The material test surfaces used in the experiment is a block of steel with mill surface machined step wedge as shown in figure 4. This gives a different surface roughness conditions to test the sensor. The experiment was performed by displacing the optical sensor laterally up to a distance of 100 mm with a speed of 5, 35 and 50 mm/s. For each speed, 5 repetitions were done to ensure the consistency of the optics performance.

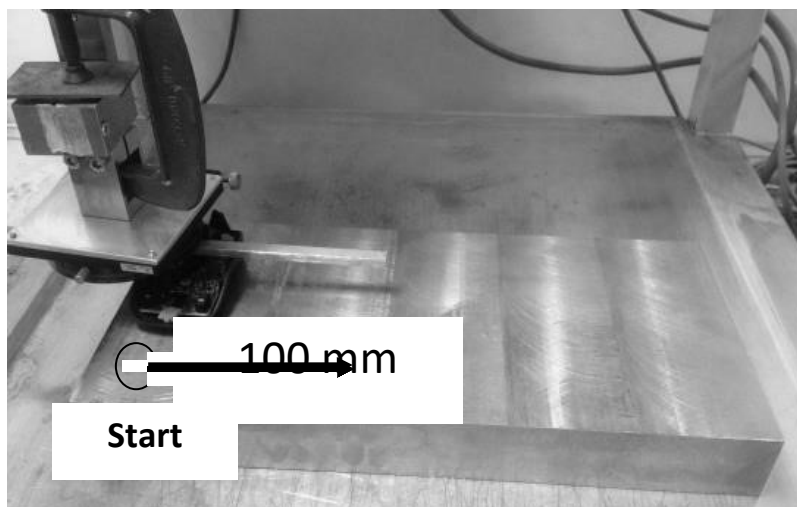


**Figure 4.** Picture of the experiment setup with the optical sensor mounted on the 3D linear stage scanner. The optical sensor is positioned on the surface of the steel - mill surface machined step wedge.

### 3.3 Optical sensor calibration test results and discussion

By performing the simple movement of the optical sensor over a known travelling distance; the measured Scaling Factor (SF) can be deduced by the following formulation,

$$SF = \frac{D_{actual}}{D_{raw}} \quad (1)$$

where  $D_{actual}$  = actual distance,  $D_{raw}$  = raw data (CPM) and  $n$  = number of tests.

Another parameter which can be determined from our analysis is the distance error which corresponds to the accuracy (Acc) of the optical sensor and this can be expressed by,

$$Acc = \frac{D_{error}}{D_{actual}} \quad (2)$$

where  $L$  = actual distance,  $L_c$  = calibrated distance and  $n$  = number of tests.

Figure 5 shows 5 individual linear displacement trajectory plots for the optical sensor performed on a steel block. The optical sensor was driven by a linear stage motor with speed of 5 mm/s and total travelled distance of 100 mm. The red circle represents the starting position which is at coordinate (0, 0). As expected, deviation from a straight line was observed at a position of around 75 mm from the start, which coincides with the step change of the steel wedge for all the 5 measurements. The deviation on the y-axis (about 3.3 mm) is due to the misalignment of the axes between the optical sensor and linear stage motor. Nonetheless, the trajectories show a relatively straight line has been moved for all the 5 measurements and stop close to the linear stage travelled distance of 100 mm.

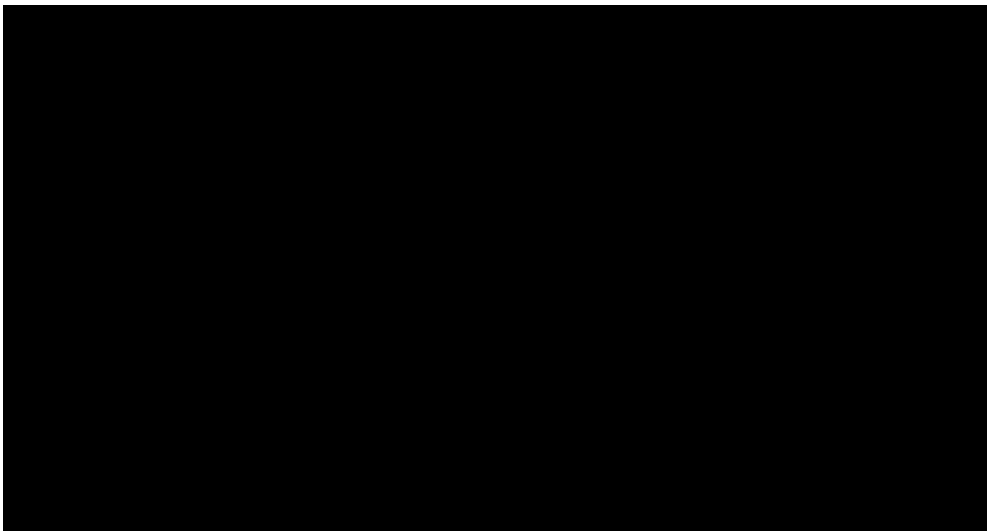


**Figure 5.** Trajectory of the optical sensor performed using a linear stage scanner with scanning speed of 5 mm/s and distance travelled of 100 mm.

Further analysis was carried to analyse laboratory results by calculating the mean and standard deviation for all the 5 measurements shown in figure 5. This is represented by the error bars (figure 6). The mean trajectory shows a change in the gradient near 75 mm as a consequence of the step change in the surface height. Clearly this demonstrates that surface quality is crucial in obtaining an accurate position. A

similar trend of the increment of standard deviation value with travelling distance increase was observed and results indicated a maximum standard deviation of  $\pm 0.2$  mm. Since the repeatability for the optical sensor has been established on the steel material, for convenience, subsequent laboratory results for varying speeds will be shown with the error bar plot.

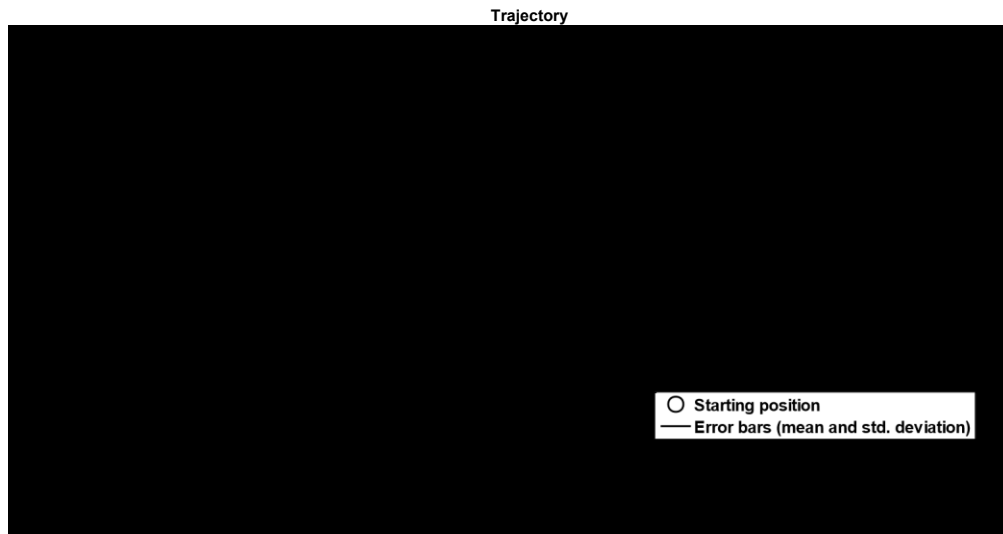


**Figure 6.** Error bars showing the mean and standard deviation for all 5 linear displacement tests performed with scanning speed of 5 mm/s and distance travelled of 100 mm.

Similarly using equations 2 and 3, the scaling factor and distance accuracy can be obtained respectively. The average of all the measurements gives an average value of 0.022 and 0.1 mm for the SF and Acc respectively which demonstrates the repeatability and robustness of the optical device.

The analysis of the experiment conducted for optical sensor travelling on the steel block with scanning speed of 35 mm/s is shown in figure 7. The mean trajectory showed a coherent change in the gradient near 75 mm as a consequence of the step change in the surface height. The maximum standard deviation observed was about  $\pm 0.15$  mm which confirms the consistency of the sensor. The SF and Acc results for the 5 linear displacement measurements yield the values of 0.022 and 0.14 mm for the average SF and Acc respectively which demonstrates the repeatability and robustness of the optical device.

Trajectory

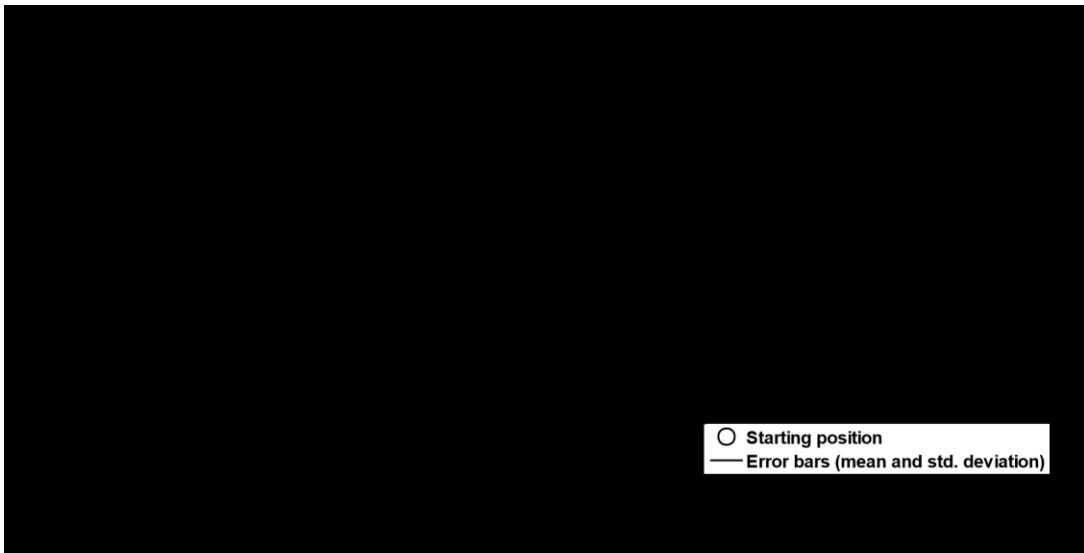


**Figure 7.** Error bars showing the mean and standard deviation values for all 5 linear displacements tests performed with scanning speed of 35 mm/s and distance travelled of 100 mm.

The scanning speed was increased to 50 mm/s (typically the maximum scanning speed for MUT) and studied in the similar fashion. Despite the speed increment to a factor of 10, good agreement of the SF and Acc results were achieved (figure 8). The maximum standard deviation was about  $\pm 0.2$  mm. The average SF and Acc yielded similar values of 0.022 and 0.114 mm respectively. Clearly, these experiment results show that the response of the optical sensor is independent of speed within the speed range used for MUT.

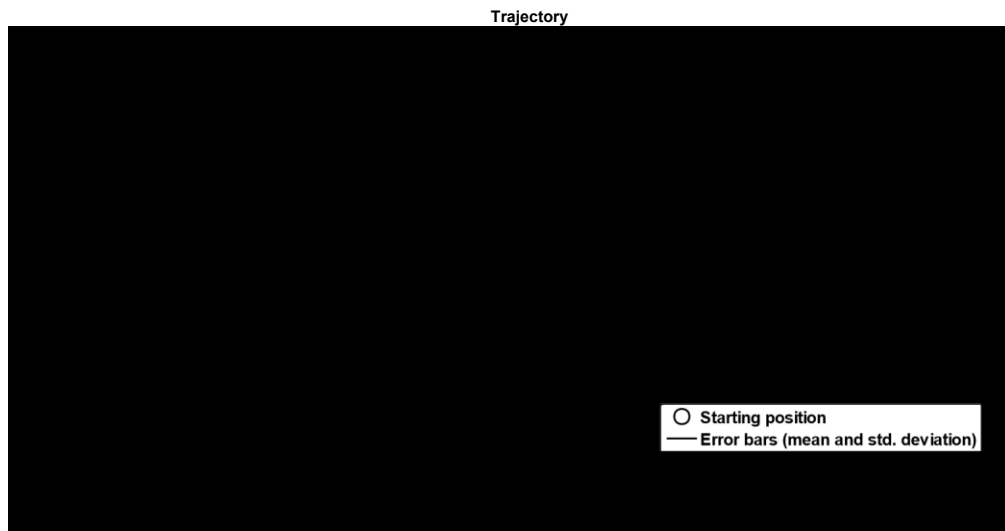


**Figure 8.** Error bars showing the mean and standard deviation values for all 5 linear displacement tests performed with scanning speed of 50 mm/s and distance travelled of 100 mm.

Subsequently, further experiments were performed for a wide variation of scanning distances for the steel block using the same experimental procedure described above. The scanning distance was taken for 50, 75, 100 and 200 mm for speeds of 5, 35 and 50 mm/s. The average (Avg.) scaling factor and

accuracy for all the individual measurements are tabulated in table 1. Encouragingly, the final average Acc for all the measurements yielded 0.094 mm for the steel block. The calibrated SF parameter of 0.023 is used to develop the STE system to be used on such material.

**Table 1.** Scaling factor and distance error for each individual optical displacement test performed on a steel block using a linear stage scanner with scanning speed of 5 to 50 mm/s and distance travelled up to 200 mm.

Measurements (Speed (mm/s), distance(mm))	Avg. SF	Avg. ACC (mm)
5, 50	0.021	-0.039
5, 75	0.022	0.062
5, 100	0.022	0.17
5, 200	0.027	0.37
35, 50	0.021	0.038
35, 75	0.022	-0.009
35, 100	0.022	0.136
35, 200	0.025	-0.023
50, 50	0.021	0.064
50, 75	0.022	-0.025
50, 100	0.022	0.114
50, 200	0.026	0.27
Final average	0.023	0.094

### 3.4. STE probe packaging design and system integration

The portability of an MUT system is regarded as one of the important considerations and the proposed integrated sensor system consists of an ultrasonic probe, optical sensor, Arduino BT and battery. The ultrasonic probe consists of a 4 MHz normal compression wave probe with 10 mm diameter served as the object to be tracked. The optical sensor and Arduino BT are powered by a 3.7 V rechargeable single cell battery with 1000 mAh capacity. For robustness, the prototype of the STE probe casing was manufactured with aluminium and Teflon. The design takes the ergonomic factor such as introducing grooves to encourage the familiar grip found in manual NDT. The complete design showing the internal arrangement can be seen in figure 9(a). The overall dimension is (LxWxH) is 162 x 60 x 40.5 mm. An initial prototype for the STE probe is shown in Figure 9(b) and (c).

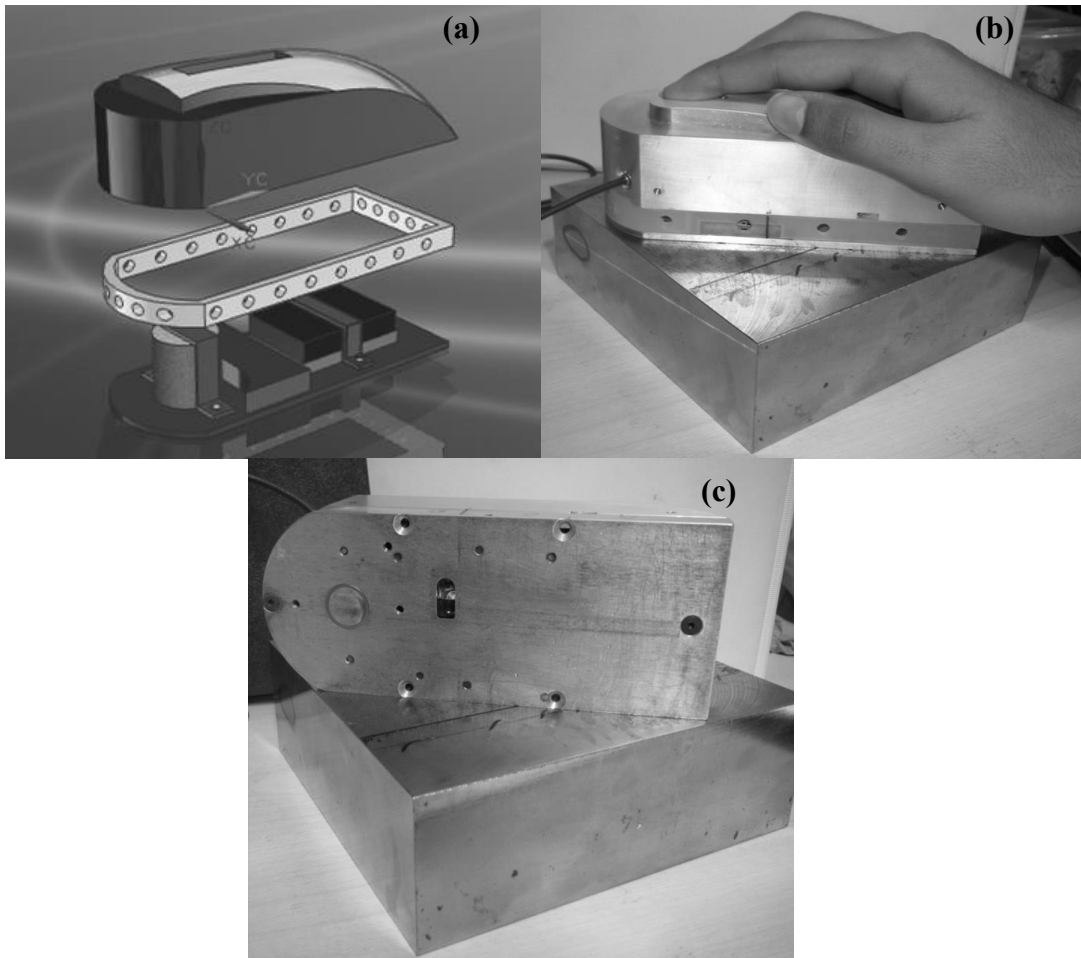


**Figure 9.** (a) Exploded view of the STE probe prototype. (b) STE probe prototype holding with one hand over a test steel block sample (side view) and (c) bottom view showing the ultrasonic probe and the optical sensor. Probe overall dimension is (LxWxH) is 162 x 60 x 40.5 mm.

The UT data is acquired by means of an US-Key pulser/receiver which supports 12 bit resolution allowing the software to configure different setting such as gain levels and gating. The amplitude of the ultrasonic signals is obtained from the stored A-scan data for each location and displayed on the screen whereas the surface coverage is shown in the form of a C-scan. A typical inspection setting using the STE and display of a complete inspection are shown in figure 10(a) and (b) respectively.

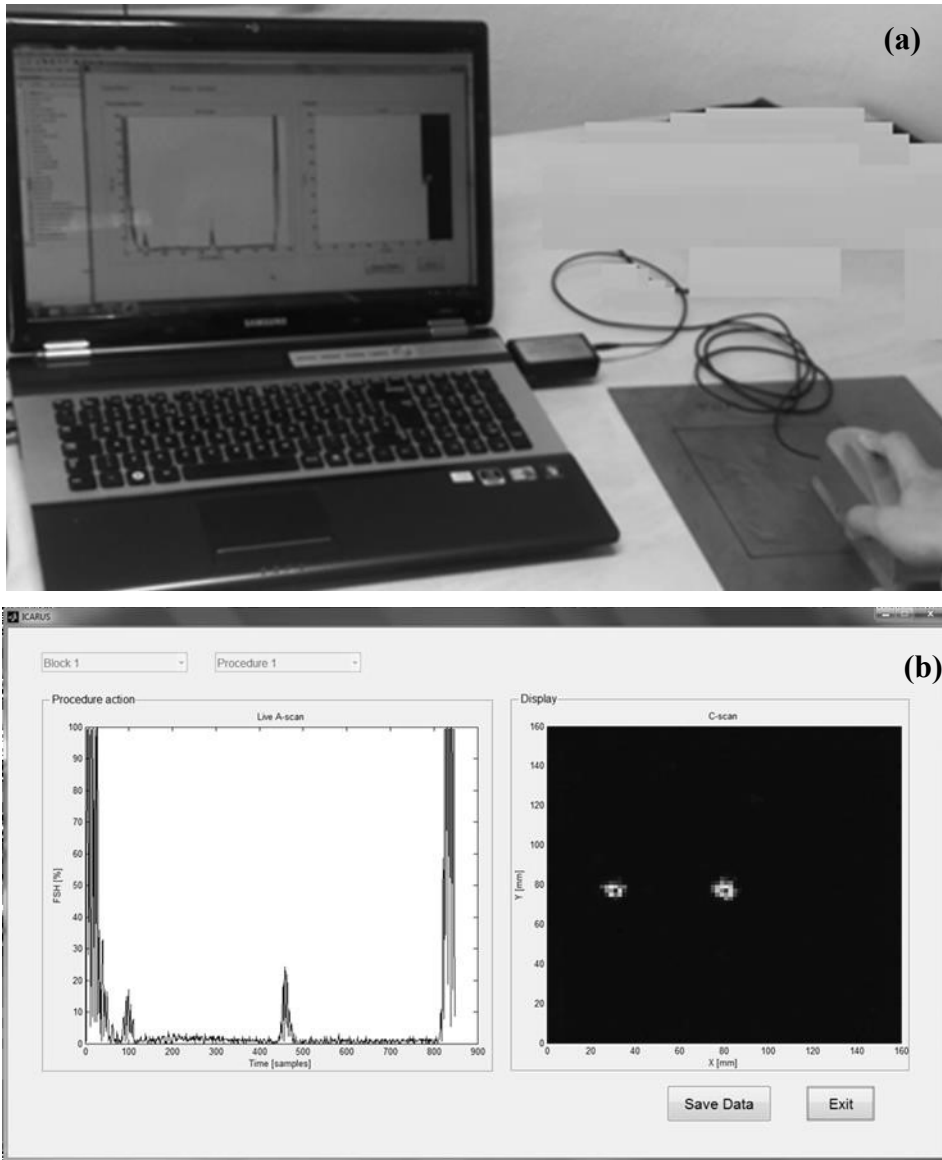


**Figure 10.** (a) A typical example using the STE for training MUT operators simulating inspection of steel and (b) display of live A-Scan signal and real time C-Scan image during the inspection.

#### 4. Trial experiments

The STE library contains a series of scenarios obtained by means of automated immersion UT scanning inspections. The test pieces are made from steel material which has flat geometry comprising Flat Bottom Holes (FBHs) of different depths and locations. Examples of test pieces in the STE library and their respective immersion UT C-scan image data are illustrated in figure 11(a) & (b) and 12(a) & (b). It is worth noting that the immersion UT system performs a scan of 5 mm excess from the perimeter of the test sample in order to make a distinction at the boundaries.

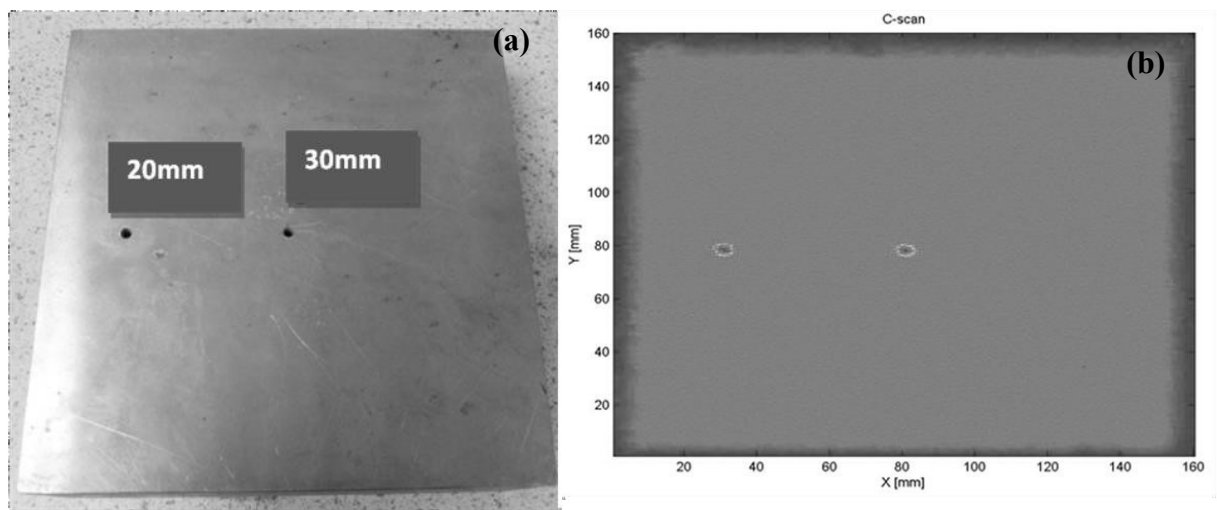


**Figure 11.** (a) Flat steel block 1, VB1 (150 x 150 x 50 mm). Two 3 mm (diameter) FBHs at 20 mm and 30 mm deep located at (25 mm, 75 mm) and (75 mm, 75 mm) respectively. (b) Corresponding C-scan image.

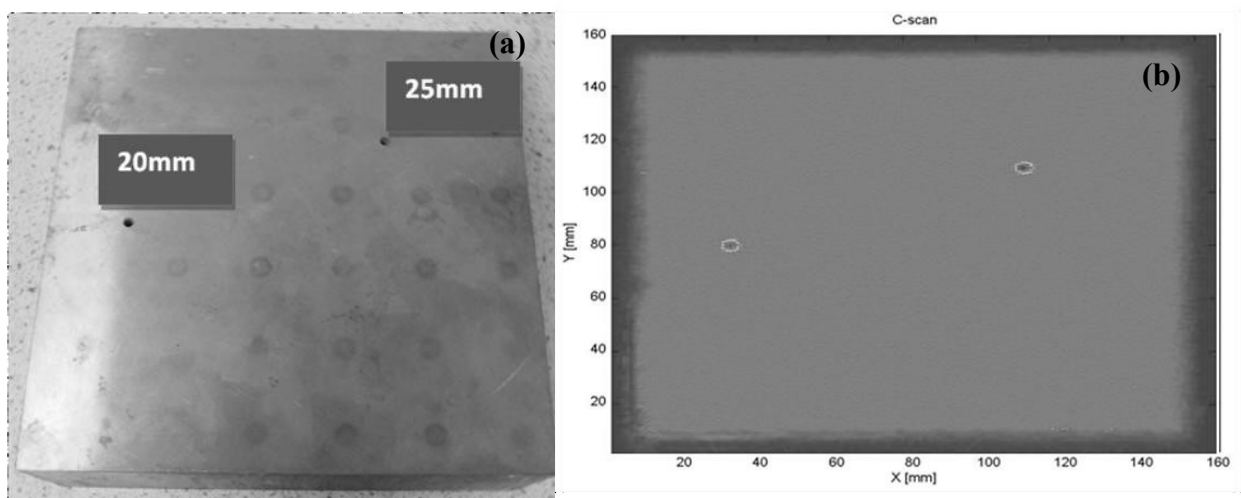


**Figure 12.** Flat steel block 2, VB2 (150 x 150 x 50mm). Two 3 mm (diameter) FBHs at 20 mm and 25 mm deep and located at (25 mm, 75 mm) and (105 mm, 105 mm) respectively. (b) Corresponding C-scan image.

A range of participants with differing levels of experience and qualifications were selected to perform MUT inspections using the STE system. The participants selected included a group of 3 personnel (U1 to U3) with no prior experience of MUT and a group of experienced operators (Q1 to Q3), possessing a range of qualifications including UT level 2 and 3. Participants were briefed on how to operate the system and were also given time to familiarise with the system (approximately 15 minutes) before commencing the test. However, the type and number of flaws were not revealed to them. In this part of the trial, participants were required to perform inspections on both virtual test pieces. It is important to note that so long as a representative geometry of the work space is used, the intrinsic material properties or thickness of the work space will not influence the performance of the STE system. An area of 160 x 160 mm was marked out for the work space which indicates the boundary to be scanned.

Each participant first selects the virtual flat steel block 1 (VB1) from the STE system user interface and steps through the procedure, explained in figure 2, displayed on the screen. For the test to be realistic, the participants were instructed to apply a thin film of water on the test surface to act as couplant for the ultrasonic probe. The probe was placed at a reference point (bottom right corner) in the marked out testing area (as shown in figure 10(a)). Each participant proceeded to scan the marked out area intending to locate the flaws within each virtual test piece. The C-scan showed the updates in real time during the scan and to aid the participants, a crosshair following the current location of the probe is simultaneously shown on the screen. A suspected defect will cause the pixel in the C-scan associated with the current probe location to change to a red colour based on the amplitude of the reflector signal in the gated region of the A-scan. Once the scan is completed, the participants will complete a reporting sheet by marking the location of the defect, a reporting sheet was completed by the participants to mark the defects shown on the C-scan data. The error can be confirmed by checking the A-scan at the location on the screen as well. The timing will be taken once the participant completed the report. This procedure is repeated for virtual flat steel block 2 (VB2).

## 5. Results and discussion

The PoD is calculated to determine the performance of the participants. PoD can be expressed by the following expression:

$$\text{PoD} = \frac{\text{Number of defects detected}}{\text{Total number of defects}} \times 100\% \quad (4)$$

The trial results are shown in figure 13 where the error deviation (i.e. distance difference between the measured and actual location of defect) is plotted against each flaw for the individual participants. The results are encouraging as all participants passed the synthetic training trial, finding all flaws (POD = 100%) in both virtual blocks to an accuracy of less than 10 mm. For VB 1 (shown in figure. 13(a) and (c)), a trend (with the exception of participant Q1) can be observed in the trial for both participant groups where the deviation error increased from the first to the second flaw. This may be attributed to the longer distance the probe has to travel from flaw 1 to flaw 2. For VB 2 the unqualified group managed to improve their performance as observed by the smaller error deviation achieved in both flaws. On the contrary, participants Q2 and Q3 of the qualified group had deteriorating performance during the scan. It is worth noting that 14 out of 24 defects found have managed to achieve an accuracy of less than 5 mm error and all defects were detected within 10 mm. It is also interesting to note that although keeping the heading of the probe seems to be quite difficult to achieve in real inspection, the trial results have demonstrated that with some practice for the trainee, reasonably good results could still be achieved. The time taken for all participants to complete each scan is approximately 10 minutes.

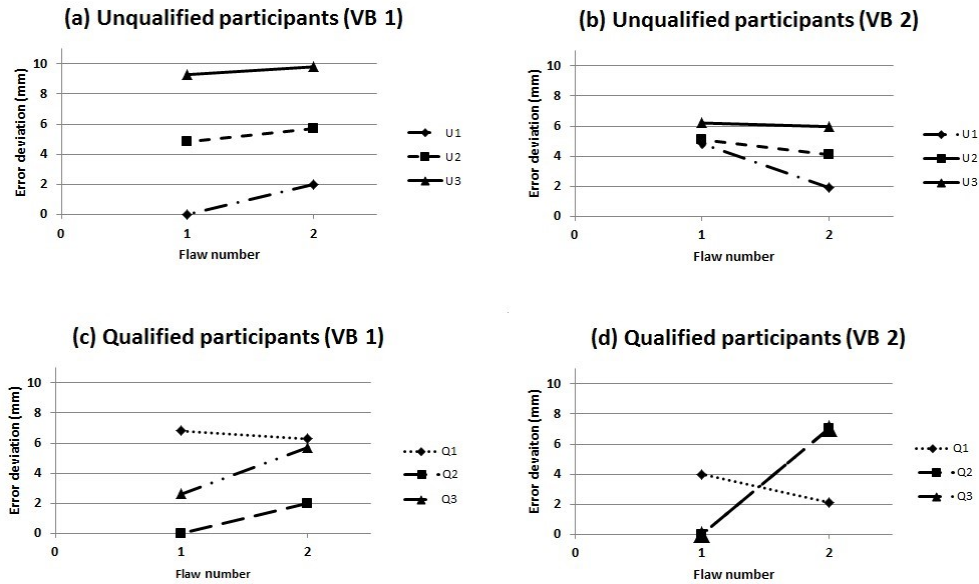


**Figure 13.** Results for distance error for the virtual training trial performed by unqualified (a and b) and qualified (c and d) participants on virtual flat steel blocks 1 (VB 1) and 2 (VB 2).

## 6. Conclusion

STE system is designed for training operators to improve their spatial dexterity skills and assessing their ability to fully cover the inspection surface. In addition, it provides electronic substitutes for real specimens and assess the operator performance where traditional training or examination methods fall short. It offers both the examiner and the trainee with additional information on how to sustain a good performance. The system also includes a library of virtual test pieces in a form of raw ultrasonic data indexed by location across the entire region of interest. A dead reckoning approach spatial positioning system has been developed for the STE system. The optical sensor was studied and tested for its capability to function as a two axes displacement sensor. The laboratory results for the positioning module shows an error of 0.05% (i.e. 0.1 mm over 200 mm) using the current optical positioning system on steel surface. This error takes account of both systematic and non-systematic errors for the optical sensor. Interfacing between the optical positioning system and the STE operating system has been achieved through the use of a wireless Arduino data acquisition board. The operating system synchronises positional information with ultrasonic data and display the corresponding C-scan map. A test bed trial using both qualified and unqualified participants has been conducted using the STE system. The trial results show a 100% POD (i.e. all 4 defects found) is achieved for all the participants with inspection time of approximately 10 minutes for each virtual test piece. The maximum distance error was contained within 10 mm for all defects where more than 50% of the measured defect locations achieved an accuracy of 5 mm. It is envisaged that this figure can be improved using a probe heading correction technique [23].

## Acknowledgements

The research leading to these results has received funding from the European Union's Seventh Framework Programme managed by REA-Research Executive Agency (FP7/2007-2013) under grant agreement number 262664. The ICARUS project is a collaboration between the following organisations: Brunel University, University College London, TWI Limited, Plant Integrity Limited, Innovative Technology and Science Limited, Vermon SA, Polkom Badania Sp ZOO, INNORA Robotics & Automation Limited and NDT Expert.

## References

- [1] Alexiev A I and Mihovski M 2000 Human Reliability in Ultrasonic *15<sup>th</sup> World Conf. of NDT* (Rome, Italy)
- [2] McGrath B, Worrall G and Udell C 2006 Programme for the Assessment of NDT in Industry 3 (PANI 3) *HM Government, Health and Safety Executive*
- [3] Stelwagen U 1995 Non-Destructive Testing of Thin Plates *Nederlands Instituut voor Laastechniek Doc 93 – 40*
- [4] 2005 Structural Integrity Analyses - Does NDT Tell Us What We Need To Know? *Structural Integrity Technical Group, TWI*
- [5] <http://www.pqndt.com/resources.html> (last accessed on 06/05/2014)
- [6] 2009 CSN EN 4179: Aerospace Series – Qualification and approval of personnel for non-destructive testing
- [7] 2008 NAS 410 Rev. 3: NAS Certification & Qualification of Nondestructive Test Personnel
- [8] Harris D H and Spanner J C 1998 Virtual NDE Operator Training and Qualification *1<sup>st</sup> International Conference on NDE - Relation to Structural Integrity for Nuclear and Pressurised Components* (Amsterdam, Netherlands) 4 10
- [9] Burch S F and Stow B A 2008 Computer Modelling of the Computed Radiographic Inspection of Wall Loss Flaws in Pipes for Image Simulation and POD Predictions *47<sup>th</sup> Annual British Conf. on NDT* (Shrigley, Cheshire)
- [10] Murgatroyd RA 1994 Human Reliability in Inspection *Results of Action 7 of PISC III Programme*
- [11] Turnbow M L 2008 Performance Based Qualification for NDT *Proceeding of the 17<sup>th</sup> World Conf. on Nondestructive Testing* (Shanghai, China)
- [12] Turnbow M L and Thompson J 2009 Reliability of NDE - the Criticality of Procedures and Personnel *4<sup>th</sup> European-American Workshop on Reliability of NDE* (Berlin, Germany)
- [13] Felice M 2012 New Ultrasonic Test Pieces for Complex Cracks *Aerospace NDT Symp.* (Bristol, UK)

- [14] Haritos T and Macchiarella D N 2005 A mobile Application of Augmented Reality for Aerospace Maintenance Training *Proc. of the IEEE 24<sup>th</sup> Digital Avionics Systems Conf.* (Washington, D.C, USA) 5.B.3:1 – 9
- [15] Crescenzo F D, Fantini M, Persiani F, Stefano L D, Azzari P and Salti S 2011 Augmented Reality for Aircraft Maintenance Training and Operations Support *Proc. of the IEEE Computer Graphic and Application* **31** 96 – 101
- [16] Dowling W D, Golas K C, Porter S M, Micheletti J D, Burkhardt G L, Fisher J L and Cobb A C 2009 Innovative NDE training, simulation, and performance improvement technologies and applications *Proceeding of the 7<sup>th</sup> Int. Conf. on NDE in Relation to Structural Integrity for Nuclear and Pressurized Components* (Yokohama, Japan)
- [17] Bosch T, Lescure M and Roviras D 1992 The physical principles of wavelength-shift interferometric laser range finders *J. Opt.* **23** 117 – 23
- [18] Wang M and Lai G M 2001 Displacement measurement based on Fourier *Rev. Sci. Instrum* **72** 3440 - 45
- [19] Higurashi E, Sawada R and Ito T 1999 Monolithic-integrated micro-laser encoder *Appl. Opt.* **38** 1746 - 51
- [20] <http://www.logitech.com/en-us/mice-pointers/mice/g9x-laser-mouse> (last accessed on 06/05/2014)
- [21] 2010 *Optical mice and how they work*, Avago technologies
- [22] Brosnan M J and Xie T 2006 Error corrected optical navigation system. US Patent. **7**; 119: 323 B1
- [23] Bonarini A, Matteucci M and Restelli M 2005 Automatic error detection and reduction for an odometric sensor based on two optical mice *Proc. of the IEEE Int. Conf. on Robotics and Automation* (Barcelona, Spain)
- [24] 2012 ADNS-5090 datasheet: Low power optical Mouse sensor, *AVAGO technologies*
- [25] <http://www.martijnthe.nl/2009/07/interfacing-an-optical-mouse-sensor-to-your-arduino/> (last accessed on 06/05/2014)